LiDARs detected signal and Target distance estimation: measurement errors from Target reflectance and multiple echos

LiDARs detected signal and Target distance estimation: measurement errors from Target reflectance and multiple echos

1st Davide Cassanelli
Dep. of Engineering "E. Ferrari"
University of Modena and R. Emilia
Modena, Italy
davide.cassanelli@unimore.it

2st Stefano Cattini
Dep. of Engineering "E. Ferrari"
University of Modena and R. Emilia
Modena, Italy
stefano.cattini@unimore.it

3st Giorgio Di Loro
Dep. of Engineering "E. Ferrari"
University of Modena and R. Emilia
Modena, Italy
giorgio.diloro@unimore.it

4st Luca Di Cecilia
CNH Industrial
Modena, Italy
luca.dicecilia@cnhind.com

5st Luca Ferrari
CNH Industrial
Modena, Italy
luca.ferrari@cnhind.com

6st Luigi Rovati
Dep. of Engineering "E. Ferrari"
University of Modena and R. Emilia
Modena, Italy
luigi.rovati@unimore.it

***Abstract*—The use of LiDARs in automotive is increasingly widespread. In order to operate in a critical environment such as that of mobility, these systems must offer increasingly high performance. In particular, the ability to estimate the position of objects regardless of their reflectance and presence of diffusing backgrounds is a very sought-after feature by manufacturers. In commercial systems various strategies are used to make the measurement as insensitive as possible to these effects, however, it is not possible to fully compensate for the measurement errors caused by them. In this paper, we propose two simple experimental setups to verify the presence of these measurement errors in two scenarios. Moreover, we report the performance of a commercial LiDAR (MRS 6000 by Sick) using certified reflectance standards (Spectralon® Diffuse Reflectance Standards, by Labsphere). For this LiDAR, the results obtained show that a logarithmic variation of the reflectance of the target of 1.26-log at a target distance 2.4 m provides incompatible measurements. Furthermore, the presence of a background at a distance shorter than 11 cm, 12 cm and 13 cm respectively with 50 %, 75 % and 99 % reflectance also provides incompatible measurements for a target distance of 1.3 m from the LiDAR.**

***Index Terms*—Laser radar, LiDAR, Reflectance, Automotive, Sensor phenomena and characterization**

I. Introduction

Autonomous driving is considered the future of automotive, both for the mobility of people and goods. Consequently, many different sensors have been developed in recent years to fulfil the strong demand for ADAS systems. Among these, LiDARs systems are distinguished for providing the environmental sensing mandatory for autonomous driving. The increasing number of products on the market raises the need to characterize their performances and capabilities to select suitable systems for specific applications. This has led and is leading to the publication of many studies aimed at the characterization and comparison of LiDAR systems [1]–[6]. Furthermore, several studies aimed at evaluating LiDARs performances in the detection of pedestrians and objects have been proposed in recent years e.g. [7]–[9]. For example, for the implementation of autonomous driving, an ADAS system must be able to recognize rubble or grit on the road surface, which can have different optical properties, e.g the reflectance. In agriculture, it is also required to recognize small objects with a large background behind them, e.g. detecting a stalk of wheat in a field. Considering this aspect, the optical properties of the object to be detected can affect the estimation of the LiDAR. Materials with different reflectances, for example, can be seen differently by a LiDAR.

The importance of the Target reflectance is well-known. Indeed, manufacturers often declare the maximum scanning range based on the reflectance of the Targets. In this regard, studies reporting the reflectance of classic objects that can be found in the automotive field to optimize the choice of ADAS system have been proposed [10]. Furthermore, a recent study has reported Targets placed at the same distance can no longer be detected when their reflectance falls below a specific value [11]. However, as described above, the reflectance of the Target and the possible presence of multiple echoes may not only result in the inability of the LiDAR to detect the Target but may also introduce an error in the estimate of the axial distance. To the best of our knowledge, no study has to date systematically addressed this analysis. In this regard, in this study, we propose a simple measurement method that allows evaluating both the effect of the reflectance of the Target in the case of a single echo (Target wider than the cross-section of the LiDAR beam) and the effect of the reflectances of multiple Targets in the case of multiple echoes. An example analysis was performed on a commercial LiDAR, i.e. an MRS 6000 by Sick. In the following, Section II describes the theoretical background, the measurement procedure, and the measurement setup adopted for this study. Then, in Section III, we present

the results obtained from both the tests we performed. Finally, in Section IV we conclude with some considerations and comments on the results obtained.

II. Statement of the problem and proposed measurement method

In LiDAR environment sensing, the reflectance characteristics of the Target directly affect the performances. In particular, in direct Time-of-Flight LiDARs the reflectance of the target affect the coming back echo waveform. The simplest scenario consists of a single uniform flat Target able to intercept the entire optical beam. In this simple situation, the echo signal consists of a single pulse whose amplitude depends on the average reflectance of the Target surface and its distance from the LiDAR. The waveform of the echo, on the other hand, could be much more complex when the Target does not completely intercept the optical beam. In this case, if the remaining part of the beam is reflected by other objects placed at different distances and with different reflectance characteristics, the echo waveform could be considerably complicated and the determination of the main Target distance could be non-trivial.

By way of example, Fig. 1 schematizes two possible scenarios assuming a waveform of the optical impulse generated by the LiDAR to be Gaussian. To simplify the discussion, let's assume that the Target distance is determined by evaluating the instant in which the echo signal crosses the I_{TH} threshold, i.e. leading-edge discrimination. The simplest scenario is schematized in Fig. 1(a): the Target intercepts the entire beam generated by the LiDAR and consequently, if the target surface is orthogonal to the pulse propagation direction, the waveform of the echo remains Gaussian. Note how, in the simple case of leading-edge discrimination, the Target distance estimation is influenced by the Target reflectance. In general, with the same target distance, the higher the reflectance and the shorter the time required for the echo to cross the threshold. Fig. 1(b) shows the situation in which the optical beam is only partially intercepted by the Target. In this scenario, we assumed that behind the Target there is an object capable of completely intercepting the remaining part of the optical beam. This object, which we will call background (BG) in the following, generates a second echo that may overlap the echo generated by the Target. In general, the superposition of the two echoes can result in a distortion of the Gaussian waveform and, therefore, an error in determining the crossing instant of the threshold. This error successively translates into an error in measuring the Target distance that is a function of the reflectance of the Target and BG, the distance of the Target from the LiDAR, and the distance between the Target and BG.

Manufacturers of LiDAR systems are very familiar with these measurement problems. Over the years, many analogical or numerical strategies have been developed to compensate for these errors. In any case, complete compensation is not possible, especially in complex scenarios such as those typical of driving. In the following, we propose two simple experimental setups to verify the presence of these measurement errors for the two scenarios shown in Fig. 1.

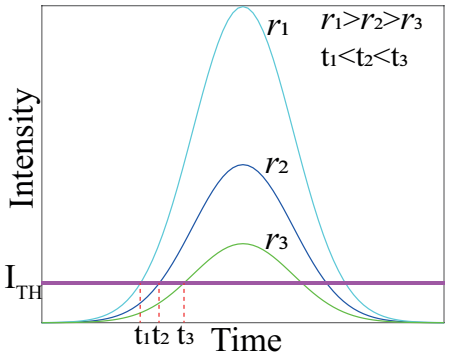

(a) Targets with different Reflectance.

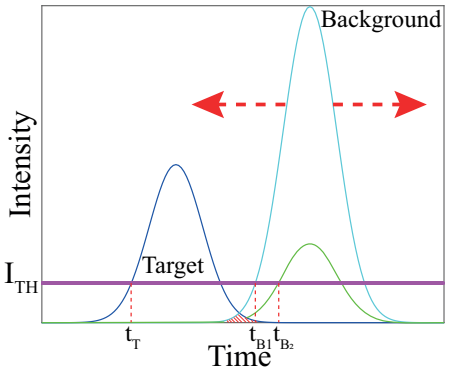

(b) Target and Background.

Fig. 1. Figure (a) shows the theoretical behaviour of three light pulses impinging Targets with different reflectances $R_1 = 2R_2, R_2 = 2R_3, R_3$. The higher the reflectance the higher the intensity. considering the pulses as Gaussian, thus reaching their peak at the same instant, it is possible to observe that the instants, t_1, t_2 and t_3, in which the pulses overcome the threshold I_{TH} are different.
Figure (b) shows the theoretical behaviour of a single beam impinging a Target with a smaller angular extension than the beam. The LiDAR receives at least two echoes coming from the Target and the background. Depending on the background reflectance and on its distance from the Target the second echoes may be received by the LiDAR at different instants (t_{B1}, t_{B2}) affecting the estimation of the Target distance. The dashed red line region shows the potential overlap between multiple echoes.

A. Single Echo

Standard reflectance Targets can be used to verify the effect of reflectance on the estimate of the Target position. The proposed measurement setup is schematically shown in Fig. 2. The instrument under test (IUT) is aligned with a sliding carriage along with a rail system. The reference Target is fixed on the sliding carriage, which enables the Target movement along the track, allowing measurement at different distances d_{Ti} for a total of N_{dist} positions. The measurement is performed analysing a single optical beam emitted by the IUT. To ensure the Target intercepts the beam of interest, the maximum distance at which the Target can be positioned

depends on the angular aperture of the IUT emitted beam and the size of the reference Target.
To perform the experimental analysis, after waiting for the warm-up time of the IUT, different reference Targets having different reflectances are placed at a known distance from the IUT and N_{rep} Point Clouds (PC) are acquired for each Target. Successively, the acquisitions are repeated at different distances.

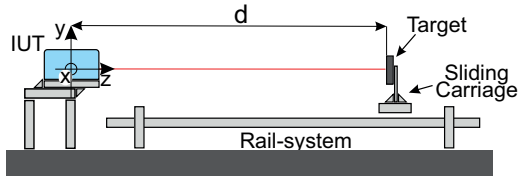

Fig. 2. Schematic representation of the the measurement setup used for the single echo analysis. IUT and Target are aligned along a rail system. The Target can be moved along the system, toward and backward the IUT, increasing or decreasing d.

Once the acquisitions have been performed, each PC is analyzed to extract the estimated distance of the Target. This operation must be carefully carried out, to ensure the correct attribution of the PC values to the Target. Selection of the PC values must take into account that the scanning LiDAR senses the environment sampling it along fixed polar directions (elevation angle ϕ and azimuth angle θ) and due to the noise, the estimated distance retrieved by a LiDAR is a random variable that can assume a value among discrete bins, whose width represents the IUT resolution $\mathcal{R}$, around the actual position of the Target [12]. Therefore, having fixed the distance d_T of the Target with known reflectance r, the mean value of the Target distance is estimated as the mean distance of the $i-th$ distance d^r_{Ti}:

$$\bar{d}^r_T = \frac{1}{N_{rep}} \sum_{i}^{N_{rep}} d^r_{Ti}. \tag{1}$$

Considering the IUT spatial resolution $\mathcal{R}$ reported in the datasheet of commercial LiDARs, type B standard uncertainty can be estimated assuming a uniform probability density function within the single bin:

$$u_B(d^r) = \frac{\mathcal{R}}{\sqrt{12}}. \tag{2}$$

B. Multiple Echoes

To simulate the presence of a second disturbing echo, a smaller Target, compared to the IUT beam size, combined with a background capable of intercepting the entire remaining part of the IUT beam are used. The proposed measurement setup is schematically shown in Fig. 3. The instrument under test (IUT) is aligned with a sliding carriage along with a rail system. The reference Target is fixed on the sliding carriage, which enables the Target movement along the track, allowing measurement at different distances d_T. Only a small portion of the beam emitted by the IUT is intercepted by the Target while a large background, placed at the distance $d_T + d_{T-B}$, intercepts the entire remaining part of the beam. To verify the dependence of the Target estimated distance on the Target position and mutual distance between the Target and BG distances d_T and d_{T-B} can be varied over the rail system. Obviously, the Target must not intercept the entire beam, constraining a minimum value for d_T, while the beam must entirely be intercepted by BG, constraining the maximum value for $d_T + d_{T-B}$. The background object BG is realized using a standard reflectance Target with known reflectance r to verify the dependence of the measured Target position on BG reflectance r. After the warm-up time, the first BG is placed on the sliding carriage behind the object. Then the BG is moved from $d_{T-B} = d_{start}$ to $d_{T-B} = d_{end}$ with step of d_{step} for a total of N_{dist} positions. At each position of the background N_{rep} PCs are acquired. This operation is performed with all the backgrounds with reflectance r known. As in the case of a single echo, according to 1 and 2, the mean value of the Target distance is estimated as the mean of the IUT readings whereas the type B standard uncertainty is derived from the IUT resolution $\mathcal{R}$.

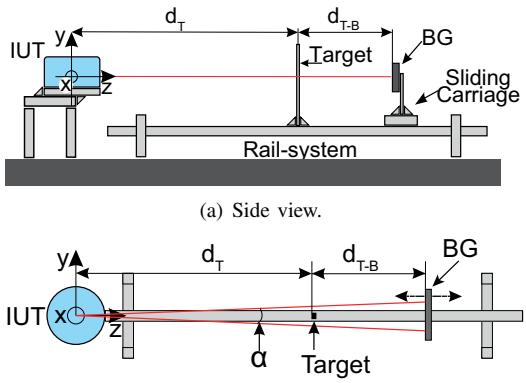

(a) Side view.

(b) Top view.

Fig. 3. Schematic not in scale representation of the measurement setup for Multiple echoes analysis. The IUT is aligned with the background and the Target along the rail system. The Target is fixed at d_T, while the background cam move in a range changing the distance d_{T-B}. The red lines represents the beam with an horizontal divergence α. The Target size has to be smaller than the beam section at d_{T-B}.

III. Results and Discussion

Using the method proposed in the previous section, the presence of residual measurement errors was verified in the case of single and multiple echos for the commercial LiDAR MRS 6000 by Sick, i.e. IUT. The wavelength of the beam emitted by the IUT was $\lambda = 870$ nm whereas its divergences were 2.1 mrad and 65.4 mrad for the horizontal and vertical directions, respectively. IUT resolution was $\mathcal{R} = 12.5$ cm [13].

A. Single echo

The Targets were realized by using 4 circular Spectralon® Diffuse Reflectance Standards, by Labsphere with radius 1 in. The certified reflectance of the Targets in the spectral range

$[250, 2500]$ nm are: $r_1 = 2$ %, $r_2 = 50$ %, $r_3 = 75$ % and $r_4 = 99$ % [14]. The acquisitions were performed at three distances from the IUT: $d_1 = 1.40$ m, $d_2 = 1.90$ m and $d_3 = 2.40$ m. Computing the size of the beam at the furthest distance of interest, i.e. $d_3 = 2.40$ m, the IUT beam spot size was (5.29 x 27.38) mm thus the Targets were able to intercept the entire IUT beam. For each Target position $N_{rep} = 100$ PCs were acquired and analyzed to extract the estimated distance of the Target according to 1.
Fig. 4 shows the obtained results. Except for the measurements acquired at $d = 2.40$ m, all the measured distances were compatible; the mean estimated distance d decreases linearly in a log-linear scale at the increase of the reflectance, for all the considered Target positions. This decreasing trend is highlighted by the red lines that represent the best linear fit of the mean values. According to the IUT resolution $\mathcal{R}$, an error bar corresponding to the type B standard uncertainty $u_B = 3.6$ cm was associated with each mean value. Slopes of the best linear fit about double as the distance of the Target increased from 1.90 m to 2.40 m indicating that the residual absolute measurement error tended to increase as the Target moves away from the IUT. Table I summarized these slopes as a function of the Target reflectance. By comparing these results with the type B IUT standard uncertainty, it is possible to observe that only in the case of $d = 2.40$ m, which manifests a 1.26-log-variations of Target reflectance, the Target distance measurements were non-compatible.

TABLE I
SLOPES OF THE BEST LINEAR FIT AS A A FUNCTION OF TARGET REFLECTANCE.

Distance of the Target (m)	Slope (mm/log(r%))
1.40	- 22.4
1.90	- 26.8
2.40	- 58.4

B. Multiple Echoes

For this experimental activity, we have chosen a Target with a reduced cross-section and low reflectance. For this purpose, we 3D printed a slab in black Polylactic Acid (PLA) of 15 mm height, 0.80 mm width and 0.2 mm thick. This Target was fixed at the distance $d_T = 1.30$ m from the IUT. The four Labsphere reference Targets used in the previous test were adopted as BG. From the Target, the BG was moved starting from $d_{T-B}^{start} = 10$ cm to $d_{T-B}^{stop} = 60$ cm with step of $d_{T-B}^{step} = 1$ cm. The size of the beam at d_T was about 3 mm by 15.5 mm, so only ≈ 27 % of the beam area was intercepted by the Target. The size of the spot at $d_T + d_{T-B}^{stop}$ was about 4.5 mm by 22 mm thus BG was able to intercept the entire IUT beam when translated between d_{T-B}^{start} and d_{T-B}^{stop}. For each BG position, $N_{rep} = 100$ PCs were acquired and analyzed to extract the estimated distance of the Target according to 1.
Figs. 5(a), 5(b), 5(c), and 5(d) shows the obtained results.

As for the previous analysis, an error bar corresponding to the type B standard uncertainty $u_B = 3.6$ cm was associated with each mean value. As shown in the figures, for all BG reflectances considered, for d_{T-B} distances greater than 30 cm, the estimated d_T value tended to a stable value, whereas d_T was increasingly underestimated as BG got closer to the Target. Observing the results, we noted that the difference D between the minimum estimation of the Target distance, i.e. when d_{T-B} was 10 cm, and its average "steady-state" value, i.e. when d_{T-B} was greater than 30 cm, tended to increase as a function of the BG reflectance. Table II resumed this difference

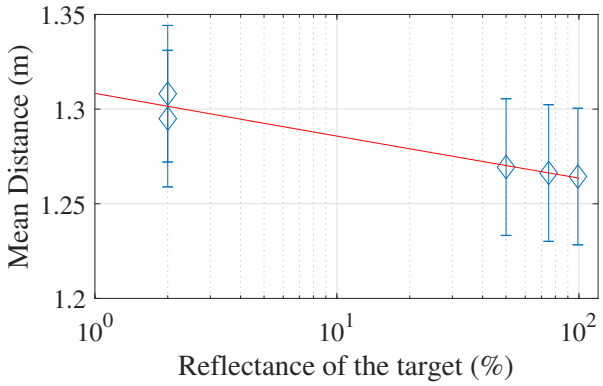

(a) Mean distance of the Target at $d = 1.40$ m.

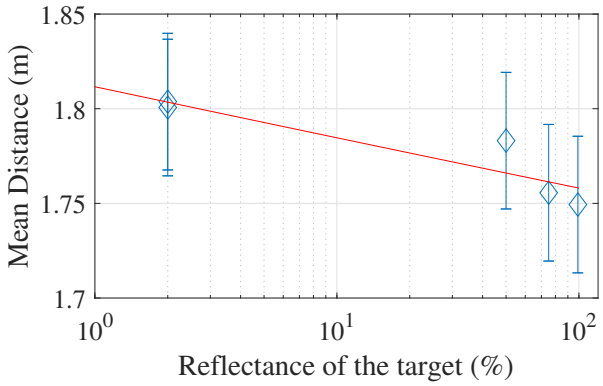

(b) Mean distance of the Target at $d = 1.90$ m.

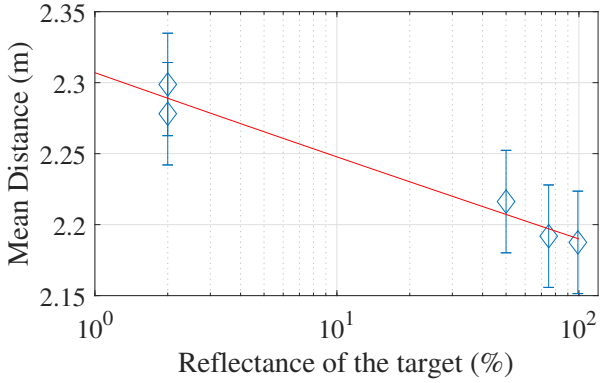

(c) Mean distance of the Target at $d = 2.40$ m.

Fig. 4. Mean estimated distance with different reflectance Target at different distances. The second acquisition at reflectance $R = 2$ % refers to the reference acquisition that shows the absence of a temporal drift in the measurement. The bars represent the uncertainty $u_B = 3.6$ cm while the red line the best linear fit. Fig.(a), Fig.(b) and Fig.(c) refer respectively to the Target fix at $d = 1.40$ m, $d = 1.90$ m and $d = 2.40$ m.

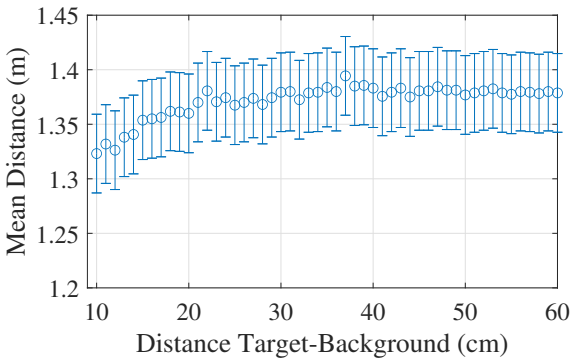

(a) Reflectance of the background $r_1 = 2$ %

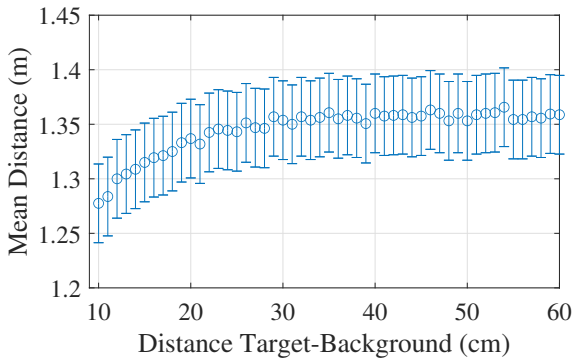

(b) Reflectance of the background $r_2 = 50$ %

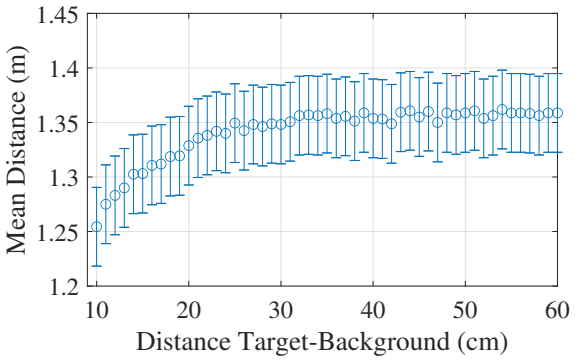

(c) Reflectance of the background $r_3 = 75$ %

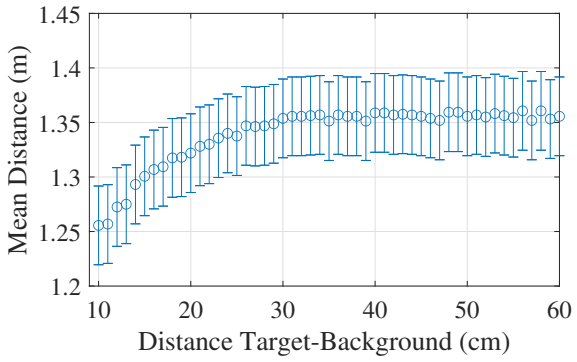

(d) Reflectance of the background $r_4 = 99$ %

Fig. 5. Estimated distance of a Target varying the distance between the Target itself and the background and the reflectance of the background. The error bars represent the measurement uncertainty type B $u_B = 3.6$ cm. Fig.(a), Fig.(b), Fig.(c) and Fig.(d) refer respectively to the background reflectance $r_1 = 2$ %, $r_2 = 50$ %, $r_3 = 75$ % and $r_4 = 99$ %.

D as a function of the BG reflectance. By comparing these results with the type B IUT standard uncertainty, it can be deduced that the presence of a background object at less than 13 cm at 99 %, 12 cm at 75 % and 11 cm at 50 % provides non-compatible Target distance measurements respect to the "steady-state" value.

TABLE II
DIFFERENCE BETWEEN THE MINIMUM ESTIMATION OF THE TARGET DISTANCE AND THE VALUE AT WHICH THE ESTIMATION STABILIZES AS A FUNCTION OF REFLECTANCE.

Reflectance (%)	D (cm)
2	5.71
50	7.97
75	10.16
99	10.01

IV. CONCLUSION

In the last decades, the automotive and mobility sectors have seen an increasingly massive use of sensors and measuring systems. Nowadays it is common to use sensors and measuring systems for driving support, monitoring specific road sections, and improving efficiency and sustainability e.g. [15]–[18]. For some sensors and measuring systems, the automotive and mobility sectors have become leading sectors of technological development. A typical example is LiDAR.

In this paper, we analyzed the effect of Target reflectance and the presence of a diffusing background on the error in the axial measure provided by LiDAR systems, analyzing the residual errors. LiDARs manufacturers adopt various strategies to reduce this type of error, but complete compensation is not possible in a complex scenario such as a typical mobility environment.

In this article, we propose a measurement method based on a simple and economical setup exploiting a rail and reflectance standards. By way of example, section III reports the results obtained applying the proposed measurement method for the analysis of a commercial LiDAR (the model MRS6000 by Sick) using certified reflectance standards (Spectralon® Diffuse Reflectance Standards, by Labsphere). The obtained results show that a logarithmic variation of the reflectance of the Target of 1.26-log at a Target distance of 2.4 m provides incompatible measurements. Furthermore, the presence of a Background at a distance shorter than 13 cm at 99 %, 12 cm at 75 %, and 11 cm at 50 % provides non-compatible Target distance measurements with respect to the "steady-state" value, i.e. when the background was at a distance greater than 30 cm.

REFERENCES

[1] S. Cattini, L. Di Cecilia, L. Ferrari, and L. Rovati, "Optical characterization of the beams generated by 3D-LiDARs: proposed procedure and preliminary results on MRS1000," *IEEE Transactions on Instrumentation and Measurement*, vol. 69, no. 10, pp. 7796–7804, 2020. [Online]. Available: https://doi.org/10.1109/TIM.2020.2984137

[2] J. Lambert, A. Carballo, A. M. Cano, P. Narksri, D. Wong, E. Takeuchi, and K. Takeda, "Performance analysis of 10 models of 3D LiDARs for automated driving," *IEEE Access*, vol. 8, pp. 131 699–131 722, 2020.

[3] F. Wang, Y. Zhuang, H. Gu, and H. Hu, "Automatic generation of synthetic LiDAR point clouds for 3-D data analysis," *IEEE Transactions on Instrumentation and Measurement*, vol. 68, no. 7, pp. 2671–2673, 2019.

[4] M. Rodriguez-Cortina, P. Adamiec, J. Barbero, X. Quintana, and M. A. Geday, "Emulation technique of multiple overlapped return echoes of a spatial LIDAR with 100-dB dynamic resolution," *IEEE Transactions on Instrumentation and Measurement*, vol. 70, pp. 1–7, 2021.

[5] D. Cassanelli, S. Cattini, G. Di Loro, L. Di Cecilia, L. Ferrari, and L. Rovati, "Comparison of VLP-16 and MRS-1000 LiDAR systems with absolute interferometer," in *2021 IEEE International Workshop on Metrology for Automotive (MetroAutomotive)*, 2021, pp. 54–59.

[6] S. Cattini, D. Cassanelli, L. D. Cecilia, L. Ferrari, and L. Rovati, "A procedure for the characterization and comparison of 3-D LiDAR systems," *IEEE Transactions on Instrumentation and Measurement*, vol. 70, pp. 1–10, 2021.

[7] T. Ogawa, H. Sakai, Y. Suzuki, K. Takagi, and K. Morikawa, "Pedestrian detection and tracking using in-vehicle LiDAR for automotive application," in *2011 IEEE Intelligent Vehicles Symposium (IV)*, 2011, pp. 734–739.

[8] J. Han, D. Kim, M. Lee, and M. Sunwoo, "Enhanced road boundary and obstacle detection using a downward-looking LIDAR sensor," *IEEE Transactions on Vehicular Technology*, vol. 61, no. 3, pp. 971–985, 2012.

[9] Z. Liu, Q. Li, S. Mei, and M. Huang, "Background filtering and object detection with roadside LiDAR data," in *2021 4th International Conference on Electron Device and Mechanical Engineering (ICEDME)*, 2021, pp. 296–299.

[10] M. Colomb, P. Duthon, and F. Bernardin, "Spectral reflectance characterization of the road environment to optimize the choice of autonomous vehicle sensors," in *2019 IEEE Intelligent Transportation Systems Conference (ITSC)*, 2019, pp. 1085–1090.

[11] S. Muckenhuber, H. Holzer, and Z. Bockaj, "Automotive LiDAR modelling approach based on material properties and LiDAR capabilities," *Sensors*, vol. 20, no. 11, 2020. [Online]. Available: https://www.mdpi.com/1424-8220/20/11/3309

[12] S. Cattini, D. Cassanelli, G. D. Loro, L. D. Cecilia, L. Ferrari, and L. Rovati, "Analysis, quantification, and discussion of the approximations introduced by pulsed 3-D LiDARs," *IEEE Transactions on Instrumentation and Measurement*, vol. 70, pp. 1–11, 2021.

[13] *MRS6000 3D LiDAR Sensor*, Sick, Waldkirch, Germany, 2019.

[14] *Spectralon® Diffuse Reflectance Standards*, LABSPHERE, INC., North Sutton, NH, US, 2019.

[15] R. Thakur, "Scanning LIDAR in advanced driver assistance systems and beyond: Building a road map for next-generation LIDAR technology," *IEEE Consumer Electronics Magazine*, vol. 5, no. 3, pp. 48–54, July 2016.

[16] J. Li, H. He, H. He, L. Li, and Y. Xiang, "An end-to-end framework with multi-source monitoring data for bridge health anomaly identification," *IEEE Transactions on Instrumentation and Measurement*, vol. 70, pp. 1–9, 2021.

[17] S. Cattini and L. Rovati, "Low-cost imaging photometer and calibration method for road tunnel lighting," *IEEE Transactions on Instrumentation and Measurement*, vol. 61, no. 5, pp. 1181–1192, May 2012.

[18] P. Ferrari, E. Sisinni, P. Bellagente, D. F. Carvalho, A. Depari, A. Flammini, M. Pasetti, S. Rinaldi, and I. Silva, "On the use of LoRaWAN and cloud platforms for diversification of mobility-as-a-service infrastructure in smart city scenarios," *IEEE Transactions on Instrumentation and Measurement*, vol. 71, pp. 1–9, 2022.